BioNanoScience (2019) 9:637–651
https://doi.org/10.1007/s12668-019-00644-w

Green Synthesis of Iron Oxide Nanoparticles Mediated by Filamentous Fungi Isolated from Sundarban Mangrove Ecosystem, India

Shouvik Mahanty[1] · Madhurima Bakshi[1] · Somdeep Ghosh[1] · Shreosi Chatterjee[2] · Subarna Bhattacharyya[3] · Papita Das[4] · Surajit Das[2] · Punarbasu Chaudhuri[1]

Published online: 11 June 2019

Abstract
In the present study, biosynthesis of iron oxide nanoparticles (IONPs) was achieved using three manglicolous fungi, STSP10 (*Trichoderma asperellum*), STSP 19 (*Phialemoniopsis ocularis*) and STSP 27 (*Fusarium incarnatum*) isolated from estuarine mangrove sediment of Indian Sundarban. Synthesised IONPs were initially monitored by UV-Vis spectrophotometer and further characterised by Fourier transform infrared (FTIR) spectroscopy, which provides information regarding proteins and other organic residues involved with iron nanoparticle. The morphology of iron nanoparticle were found to be spherical with average particle size ranging between 25 ± 3.94 nm for *T. asperellum*, 13.13 ± 4.32 nm for *P. ocularis* and 30.56 ± 8.68 nm for *F. incarnatum*, which were confirmed by field emission scanning electron microscopy (FESEM) and transmission electron microscopy (TEM). Energy-dispersive x-ray analysis (EDX) analysis was performed during FESEM study to confirm the presence of elemental Fe in the sample. X-ray diffraction (XRD) pattern has shown that the IONPs are iron oxide in nature.

Keywords Green synthesis · Manglicolous fungi · Iron oxide nanoparticles (IONPs) · Indian Sundarban

1 Introduction

In the last two decades, synthesis of inorganic nanoparticles of novel metals has attracted the attention of researchers from applied and fundamental fields [1]. Utilisation of nanoparticles of noble metals (Ag, Au, Pt); magnetic compounds (Fe_2O_3, Fe_3O_4) and semiconductors (PbS, ZnS) have shown enormous impacts in various fields of biotechnology, environment, information technology, medicine, MRI imaging and treatment of cancer [2–6]. Nowadays, iron oxide nanoparticles (IONPs) are considered as a potential candidate for environmental remediation [7, 8]. The synthesis of nanoparticle of different shapes, sizes, and chemical compositions is an interesting area for the researchers [9]. The unique catalytic [10], optical [11], electronic [12] and photochemical properties [13] of the nanoparticles contribute towards a wide range of applications in the field of applied and basic research. There are several physical and chemical processes like microwave irradiation [14], sonolysis [15] and photochemical and chemical reductions [16], which are commonly employed for the synthesis of IONPs. Most of these synthesis processes involve hazardous and expensive chemicals which brings the necessity for the development of green, environmentally benign and sustainable process for the synthesis of IONPs.

Green synthesis is an alternative, safe, eco-friendly and economic method where biological components are utilised for the synthesis of IONPs. IONPs thus generated are considered as a single domain consisting of a large surface area and shows superparamagnetic phenomenon due to quantum tunnelling, of magnetisation, which dramatically changes the magnetic property of the nanoparticles [17]. In recent years, green-synthesised magnetic nanoparticles are widely used as nanobiocides, nanocatalysts [18], nanomedicine [19], nanoadsorbent and nanofiltration [20, 21]. Different biological components like plant extract [22–24], bacteria [25], fungi [26], yeast and algae [27] commonly acts as an eco-friendly

✉ Punarbasu Chaudhuri
punarbasu_c@yahoo.com

[1] Department of Environmental Science, University of Calcutta, Kolkata, WB, India

[2] Department of Life Science, NIT Rourkela, Rourkela, India

[3] School of Environmental Studies, Jadavpur University, Kolkata, India

[4] Department of Chemical Engineering, Jadavpur University, Kolkata, India

and sustainable precursors for the green production of IONPs. IONPs synthesised by the plant extract of *Camellia sinensis* [22], *Azadirachta indica* [23] and *Punica granatum* [24] and microorganisms like *Alternaria alternata* [26] and *Chlorochoccum* sp. [27] had shown effective roles in the treatment of contaminated water. High sustainability of the microorganisms under ambient pressure, acidity and temperature renders them as a potential candidate for the development of IONPs. Among diverse group of microorganisms, fungi have been reported as a novel and effective candidate for the green production of IONPs [28–32].

In comparison to other microorganisms, fungi are easy to handle, have faster growth rate and needs low-cost maintenance, which makes them perfect organisms for the green synthesis of nanoparticles. Due to its filamentous nature, they can withstand agitation in bioreactors and can produce huge amounts of extracellular enzymes in a short period of incubation time [28], which acts as an efficient bioreductant for the green synthesis of nanoparticles [33, 34]. Although most of the reported works for the mycosynthesis of IONPs represents utilisation of terrestrial fungi [28–32], as per best of our knowledge, there is a single report where fungi isolated from a mangrove habitat was utilised for the production of silver nanoparticle [32]. Thus, exploring the potentiality of fungi isolated from a mangrove habitat for the green production of IONPs brings a novel avenue for research.

Mangrove forest consists of a detritus-based niche which serves as a hot spot for fungal diversity [35]. The Sundarbans mangrove forest is a coastal wetland which is formed by sedimental deposition by three major rivers: Ganga, Brahmaputra and Meghna [3]. It covers about 350 km (in width) of land and is shared between India and Bangladesh [36]. The fungal communities which inhabit the mangrove forests are known as 'manglicolous fungi'. They have been recognised as the second largest group of marine fungi [37]. Several environmental factors such as substrate diversity, salinity, intermittent inundation and regular interval changes of water levels due to tides contribute to species diversity in mangrove fungi [38]. Moreover, regular exposure of salt can lead to high salt tolerance in these fungi [39]. Manglicolous fungi play an ecologically important role in the mangrove ecosystem. They shows an active participation in nutritive cycle by decomposition of organic matter by production of various extracellular degradative enzymes such as amylase, cellulose, xylanase and pectinase [40]. Due to their stress tolerance capacity and being a rich source of various bioactive compounds, manglicolous fungi are considered as excellent candidate for nanoparticle synthesis.

In the present study, the novel production of IONPs was achieved with the application of three manglicolous fungi isolated from mangrove sediments of Indian Sundarbans. The article provides a detailed report on the characterisation of IONPs using various instruments.

2 Material Methods

2.1 Sampling Location

Surface sediment at 5–10-cm depth were collected aseptically from intertidal zone of mangrove wetland of Satjelia island (22° 8′ 52.12″ N, 88° 51′ 47.69″ E) located in the eastern Indian Sundarban region (Fig. 1). Collected sediment sample were kept inside a ziplock pouch in an ice box and transferred immediately to the laboratory for further processing.

2.2 Isolation of Fungi from Soil Sample and Collection of Fungal Cell Filtrate

The serial dilution and agar plating was employed for the isolation of manglicolous fungi from the sediment sample. One hundred microliters of each diluted sediment samples were inoculated aseptically on potato dextrose agar (PDA, HiMedia India) and Czapek dox agar (CDA, HiMedia India) using spread plate technique. Antibiotic ampicillin (100 μg/ml) was added to the media for checking the bacterial growth. Plates were incubated for 72 h at 28 °C (pH 5.6 ± 0.02). All reagents and culture media components ($FeCl_3$, $FeCl_2$ culture media, etc.) were purchased from Merck (India) and HiMedia Laboratories (India). Ten fungal strains were isolated from the sediment sample (Fig. 2). Preliminary identification on the basis of morphological characteristics of the fungal isolates were carried out according to their colony morphology, colour, arrangement of filaments and spore shape, following the slide culture technique and cotton blue staining [41–43]. Each fungal isolate was morphologically identified under compound microscope following the identification key present in the standard manual [41–43]. Fungal isolates were then subculture in PDA and CDA slants (pH 5.6 ± 0.02). From each subcultured tube, fungal isolates were aerobically cultured in 50-ml autoclaved potato dextrose broth (PDB) in 250-ml Erlenmeyer flask for 11 days at 27 °C (pH 5.6 ± 0.02) [34]. After 11 days of incubation period, the vacuum pump-assisted filtration of the media was done aseptically through Whatman filter paper 1. Fifty millilitres of fungal cell filtrate (FCF) was collected in sterilised 50-ml falcon tube and was centrifuged at 5000 rpm for 5 min. The supernatant were again filtered through Whatman filter paper 1. The final filtrate was collected in sterilised 50-ml falcon. FCF was later utilised for the bioreduction of salt solution comprising ferric tri chloride ($FeCl_3$) and ferric dichloride ($FeCl_2$) [29].

2.3 Synthesis of IONPs

FCF of all fungal strains were screened to check their potentiality for reduction of precursor salt solution consisting of ferric trichloride ($FeCl_3$) and ferric dichloride ($FeCl_2$) by co-

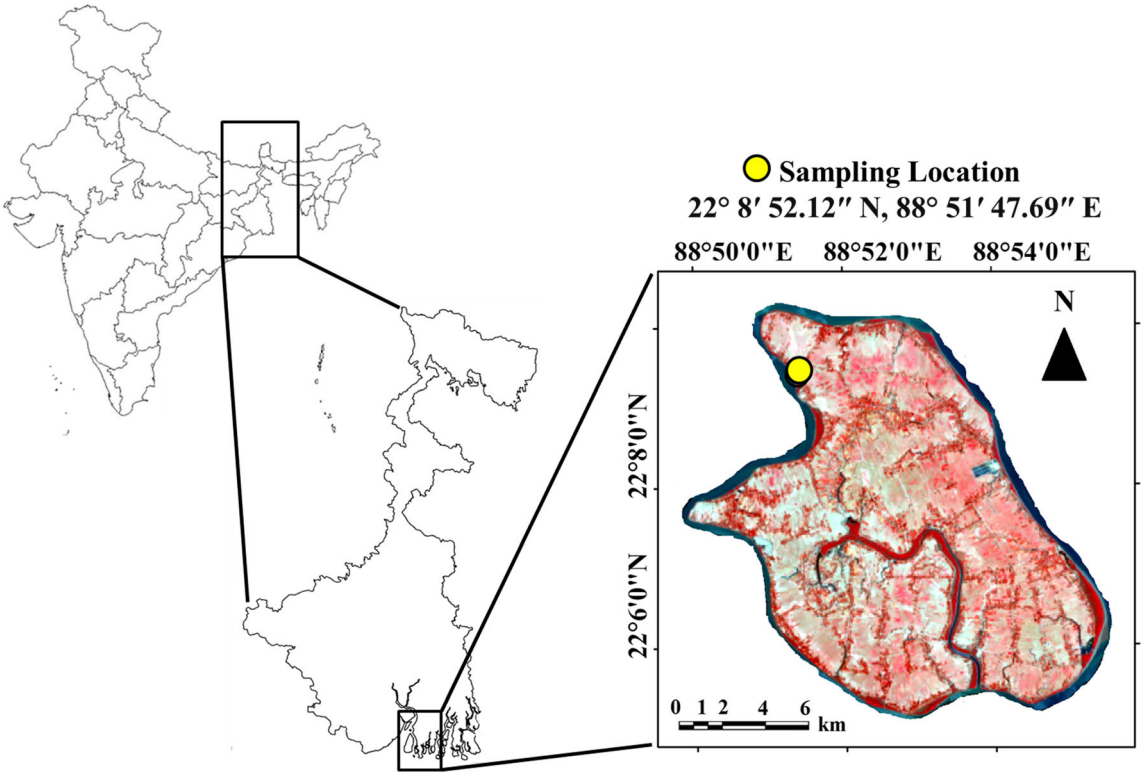

Fig. 1 Study area map

precipitation assay. Ten millilitres of FCF was mixed with solution containing ferric trichloride ($FeCl_3$) and ferric dichloride ($FeCl_2$) salt solution (2:1 mM final concentration) in 15-ml sterilised falcon tube (pH 3.2 ± 0.02). The reaction mixture was agitated for 5 min at room temperature (30 °C). The visual change in the colour of the reaction mixture was considered as positive result for the development of IONPs. The fungal strains showing positive result were further selected for molecular identification.

The formed IONPs was separated by centrifugation at 12,000 rpm for 20 min and washed thrice with deionised water. The purified IONPs were re-dispersed in the deionised water and ultrasonicated in Biobase ultrasonicate (Biobase UC20A) cleaner. The synthesis of IONPs were repeated thrice ($n = 3$) and subsequently utilised for the characterisation of particles. FCF (without precursor salt) and salt solution (without FCF) were considered as positive and negative control. Flow chart for the synthesis of IONPs has been shown in Fig. 3.

2.4 Molecular Characterisation of Fungus

Fungal DNA was extracted from the culture which has shown positive results for the synthesis of IONPs using HiPurA™ plant genomic miniprep purification kit. Quality of extracted DNA was evaluated on 0.8% agarose gel [44], a single band of high molecular weight DNA was observed. Amplification of Internal transcribed spacer (ITS) of ribosomal DNA was amplified using primers ITS1 (5′TCC GTA GGT GAA CCT TGC GG 3′) and ITS4 (5′TCC TCC GCT TAT TGA TAT GC 3′) [45]. PCR reaction was carried out in 25 μl containing ddH_2O 16.8 μl, PCR buffer (10×) 2.5 μl, dNTP's (200 mM) 1 μl, Taq polymerase (1 U/μl) 0.2 μl, Primer ITS1 (10 pM/μl) 1 μl, Primer ITS 4 (10 pM/μl) 1 μl and Template DNA 2.5 μl. The PCR reaction was carried out using Veriti® 99 well Thermal Cycler (Model No. 9902). The PCR condition followed for amplification were 5 min of initiation denaturation at 95 °C, followed by 30 cycles of 1 min of denaturation at 95 °C, annealing at 57 °C for 1.5 min, extension of 3 min and a final extension of 7 min at 72 °C The PCR amplicon was enzymatically purified and further subjected to Sanger sequencing (ABI 3730xl Genetic Analyser). Consensus sequence of ITS region was generated from forward and reverse sequence data using aligner software. Molecular identification of isolates was carried after comparison of sequences using the Basic Local Alignment Search Tool (BLAST) network services of the National Centre for Biotechnology Information (NCBI) database (http://www.ncbi.nlm.nih.gov/). The sequence data were processed using BioEdit (version 7) and most closely related species were determined. The sequences were further submitted to Gene Bank for obtaining the accession numbers.

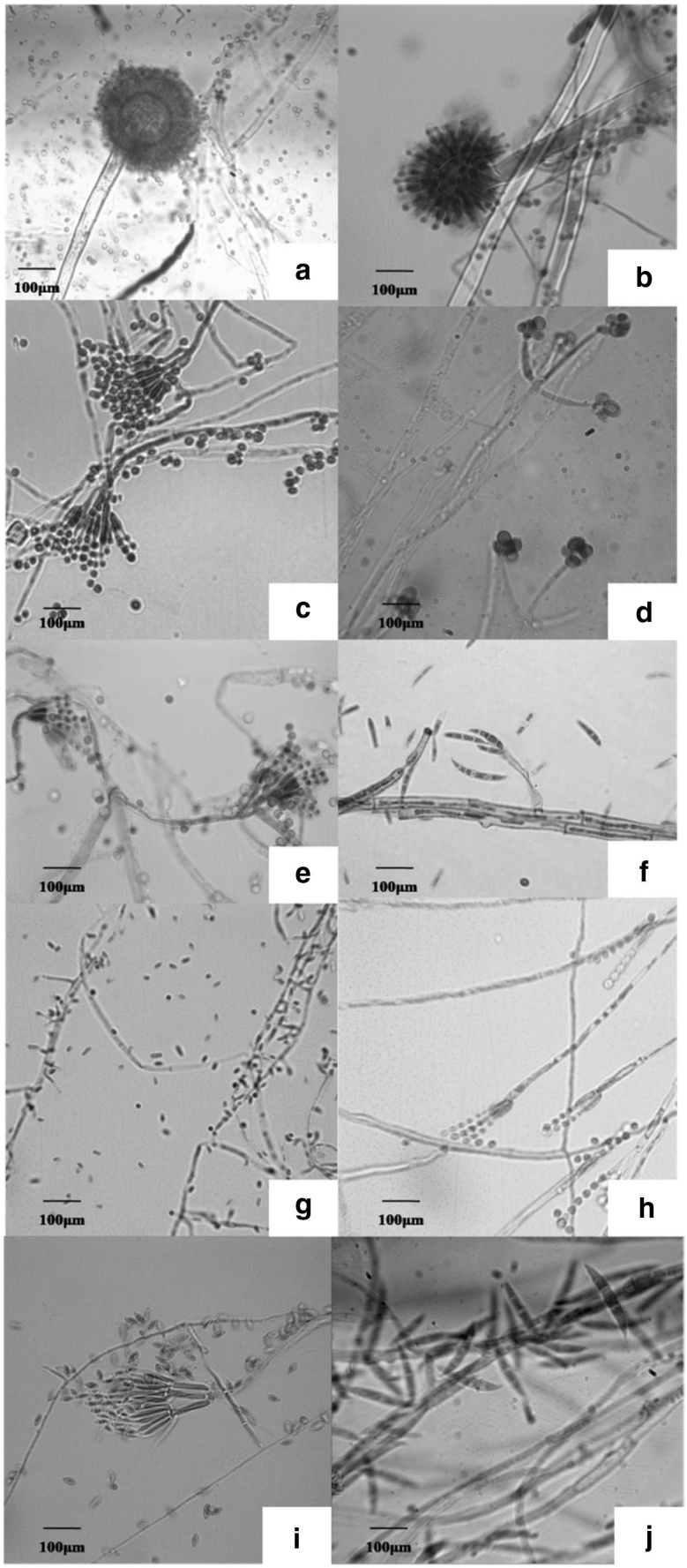
a
100µm
b
100µm
c
100µm
d
100µm
e
100µm
f
100µm
g
100µm
h
100µm
i
100µm
j
100µm

◀ **Fig. 2** Morphological characteristic of fungal isolates. **a** STSP 2 (*Aspergillus* sp.). **b** STSP 7 (*Aspergillus* sp.). **c** STSP 8 (*Penicillium* sp.). **d** STSP 10 (*Trichoderma* sp.). **e** STSP 14 (*Penicillium* sp.). **f** STSP 18 (*Fusarium* sp.). **g** STSP 19 (*Phialemoniopsis* sp.). **h** STSP 24 (*Penicillium* sp.). **i** STSP 26 (*Penicillium* sp.). **j** STSP 27 (*Fusarium* sp.)

2.5 Characterisation of the Green-Synthesised IONPs

The green-synthesised IONPs were characterised to understand their shape, size and morphology using various instruments.

2.5.1 UV-Visible Absorption Spectroscopic Analysis

The nanoparticle formed was characterised using a UV-Vis spectrophotometer system (PerkinElmer Lambda 35 UV-Vis spectrophotometer) between 200 and 700 nm with 1-nm intervals, using a quartz quavate of 1-cm thick. The progress of reaction was monitored by the visual change in colour of the reaction mixture.

2.5.2 Fourier Transform Infrared Spectroscopic Analysis

For Fourier transform infrared spectroscopic (FTIR) analysis, the lyophilised IONPs were mixed with potassium bromide at a ratio of 1:100 in attenuated total reflection (ATR) mode and the spectra were recorded with a Jasco FT/IR-6300 between 3500 and 400 cm^{-1} operating at 4 cm^{-1} resolution.

2.5.3 Field Emission Scanning Electron Microscope

IONPs in the reaction mixture were separated by centrifugation at 12,000 rpm for 20 min and washed with deionised water. IONPs suspension was then centrifuged and the pellet was lyophilised using free dryer (Biobase BK-FD10PT). Lyophilised IONPs powder samples were further analysed with FESEM (JEOL JSM-7600F) at 15–20 kV.

2.5.4 Transmission Electron Microscopic Analysis

Five microlitres of the sample solution was placed on carbon-coated copper grids and was kept in desiccators. After drying, the grids were observed in JEOL JEM 2100 HR. Evaluation of the size distribution for IONPs polydispersity index (PDI) was calculated using following equation [46, 47].

$$PDI = (\sigma/D)^2 \quad (1)$$

where D is equivalent to the mean diameter of the IONPs and the σ is equivalent to the standard deviation.

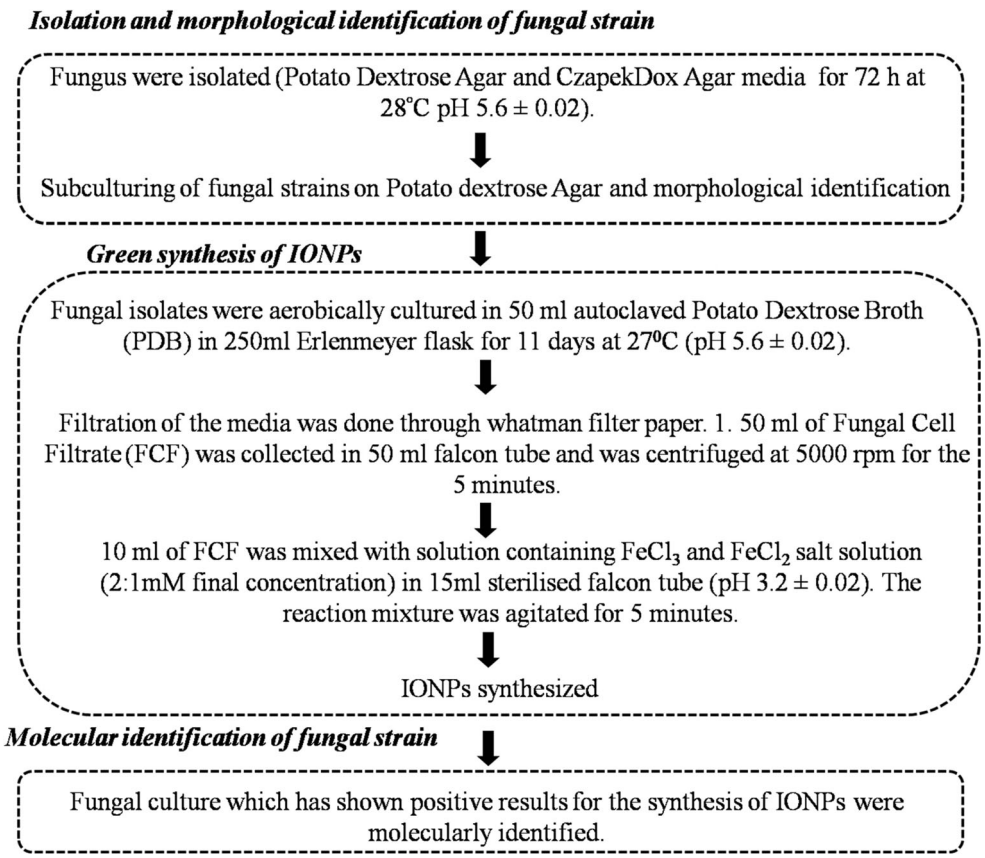

Fig. 3 Flow chart for the synthesis of IONPs

2.5.5 Energy-Dispersive X-Ray Analysis

Lyophilised IONPs was analysed with field scanning electron microscopy (FESEM; JEOL JSM-7600f FESEM) at 15 kV voltage, equipped with EDX (Oxford Instruments, INCA PENTA FET X3).

2.5.6 X-Ray Diffraction Analysis

The crystalline phase of nanoparticle was identified by x-ray diffraction (XRD) measurements carried out on x-ray diffractometer (Philips, Model: PW1830). The diffraction pattern of thin layer of synthesised nanoparticle on glass substrate was recorded from 10° to 80° (2θ) with a step size of 0.02° using Cu Ka ($k = 1.542$ Å) as radiation source and operating at 40 kV–30 mA. The crystal phase was determined by comparing the calculated values of interplanar spacing and the corresponding intensities of diffraction peaks with theoretical values from the Joint Committee on Powder Diffraction Standards-International Centre for Diffraction Data (JCPDS-ICCD) database.

3 Results and Discussion

3.1 Screening and Molecular Identification of the Potential Fungal Species

Fungi were isolated from sediment samples of intertidal zone of Satjelia island located in eastern region of Indian Sundarban. On the basis of preliminary morphological identification a total of 10 (Fig. 2) fungal strains belonging to five genus *Aspergillus* sp., *Trichoderma* sp., *Penicillium* sp., *Fusarium* sp. and *Phialemoniopsis* sp. were obtained. After screening, the fungal isolates, which had shown maximum potentiality for hydrolysing the precursor salt complex, were selected for molecular identification. FCF collected from isolate STSP 10, STSP19 and STSP27 had shown a positive result in the bioreduction of precursor salts. The visual identification of changes in colour of the reaction mixture (Fig. 4) after 5 min of incubation at room temperature (30 °C) was considered as a positive result for the formation of IONPs. The formation of IONPs might occur due to reduction of iron chloride complex by FCF following three simple steps. The first step involved release of chloride from iron chlorine complex immediately when placed in the solution [19]. In the second step, several extracellular fungal bioactive molecules like proteins, polysaccharides, enzymes and polyphenols, which constitute the FCF in the solution, acted as a hydrolysing agent and might formed a partial bond with metal ions [19, 48]. In the third step, a partial bond between the metal ion and biomolecules got broken and electrons were transferred to metal ions, further co-precipitation and nucleation of available ions results in synthesis of IONPs in the reaction mixture [19, 48, 49]. The IONPs generated was further monitored in UV-Vis spectrophotometer. In case of positive control (only FCF) and negative control ($FeCl_3$/$FeCl_2$ solution), no visual change in colour was observed. Molecular identification of fungal isolates were carried out by analysing the sequences of the ITS region of ribosomal DNA. The PCR sequencing products for ITS region resulted in 585 bp for STSP10, 540 bp for STSP19 and 550 bp for STSP27. The sequences were compared in BLAST algorithm. Isolate STS10 had shown maximum similarity with *Trichoderma asperellum*, STSP 19 had shown maximum similarity with *Phialemoniopsis ocularis* and STSP 27 had shown maximum similarity with *Fusarium incarnatum.* These fungal DNA sequences were submitted in NCBI gene bank. The accession numbers for the isolate STSP10 is MH045583, for STSP 19 is MH045585, and for STSP 27 is MH045587.

3.2 Characterisation of Green-Synthesised IONPs

3.2.1 UV-Visible Spectra Analysis of the IONPs Suspension

Optical property of green-synthesised IONP suspensions was evaluated by UV-VIS spectroscopy analysis (Fig. 5). UV-VIS spectrum of IONPs suspensions exhibited increase in the intensity of absorbance in the shorter UV spectrum. Green synthesised IONPs, synthesised by *F. incarnatum*, *T. asperellum* and *P. ocularis* had shown a maximum absorbance at 216 nm, 290 nm and 298 nm, respectively, which might be due to plasmon resonance of unoxidised iron nanoparticle [49–52]. This result shown by IONPs synthesised by *F. incarnatum* was found to complement the report provided by Mazumdar and Haloi [49]. A broad peak at 435 nm was also observed for IONPs synthesised using *T. asperellum* which might ascribe to iron (core shell) nanostructures present in the solution [50].

3.2.2 FTIR Characterisation of IONPs

FTIR spectroscopy analysis (Fig. 6) was carried out to investigate the presence of biomolecules in synthesised IONPs. The FTIR analysis of lypholised IONPs synthesised by *T. asperellum*, *P. ocularis*, and *F. incarnatum* has showed band at wavenumbers 560 cm^{-1} and 670 cm^{-1} which designates Fe–O–Fe band [53]. Band at a wavenumber of 1045 cm^{-1}, 1075 cm^{-1} and 1064 cm^{-1} for iron oxide nanoparticles synthesised by *T. asperellum*, *P. ocularis* and *F. incarnatum*, respectively, showed the C–O–C stretch band [54]. Wavenumbers 1283 cm^{-1} and 1380 cm^{-1} showed COO- stretching band [55]. Peaks observed at 1510–1545 cm^{-1} and 1635–1640 cm^{-1} indicated the presence of amide II and

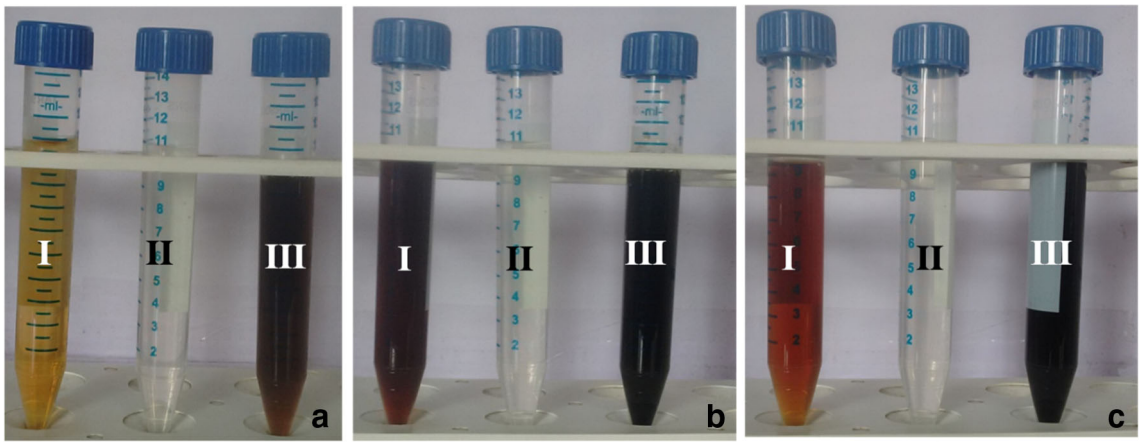

Fig. 4 FCF of fungal isolates of **a** STS10 (*Trichoderma asperellum*), **b** STSP 19 (*Phialemoniopsis ocularis*) and **c** STSP 27 (*Fusarium incarnatum*) showing colour change during reaction with iron precursor salts. I = FCF (positive Control), II = iron precursor salt (negative control), III = Appearance of black colouration due to addition of FCF to 2:1 M ratio of $FeCl_3$ and $FeCl_2$ solution after 5-min incubation

amide I bond, respectively, for all the green synthesised IONPs, which could suggest involvement of extracellular protein in synthesis of nanoparticles [56]. The peak at wavenumber 3385 cm^{-1} showed the OH stretch band which suggested the involvement of water molecule due to exposure of IONPs in air during sample analysis [57].

3.2.3 Field Emission SEM TEM Analysis of IONPs

Iron salts were biologically reduced to form IONPs by three manglicolous fungal species *T. asperellum*, *P. ocularis* and *F. incarnatum* were characterised using FESEM and TEM which showed the spherical nature and different sizes of nanoparticles

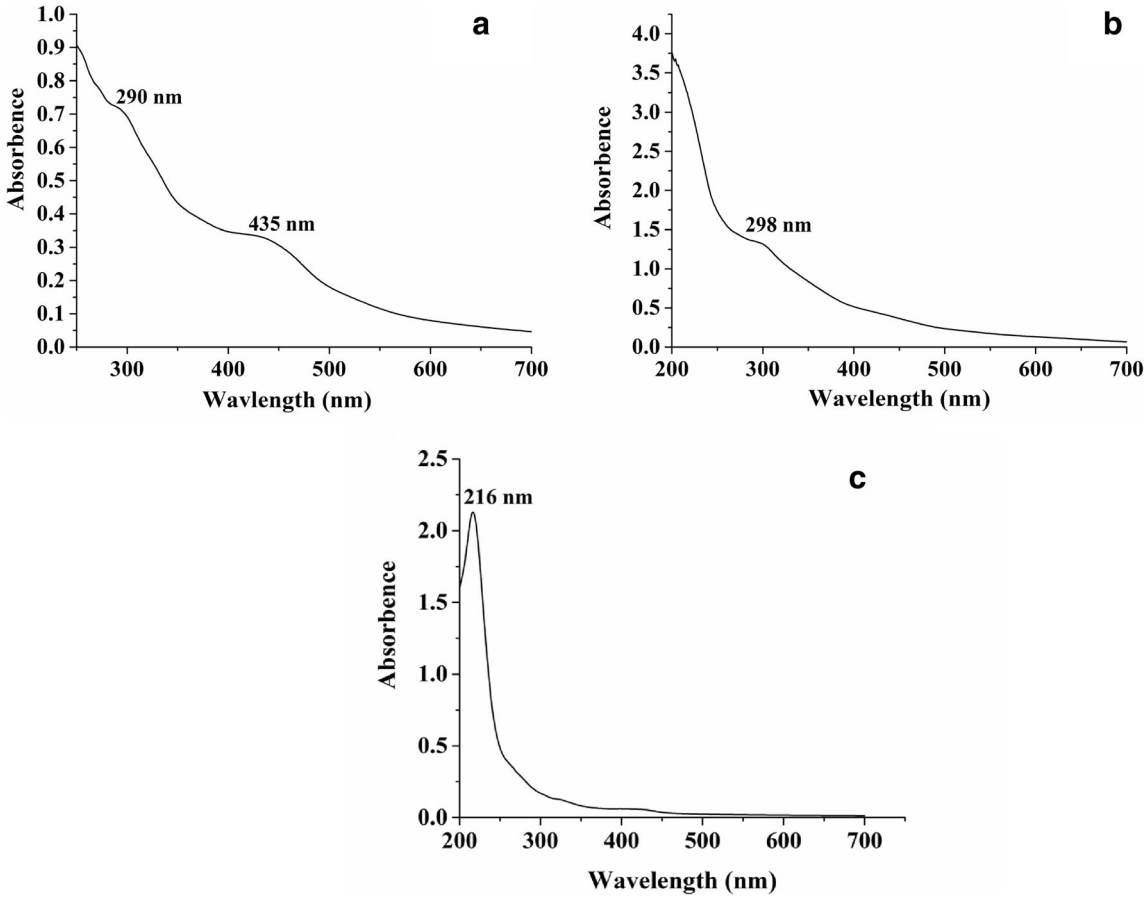

Fig. 5 UV-Vis spectra of IONPs in aq. solution synthesized by fungal isolates. **a** STSP10 (*Trichoderma asperellum*). **b** STSP 19 (*Phialemoniopsis ocularis*). **c** STSP 27 (*Fusarium incarnatum*)

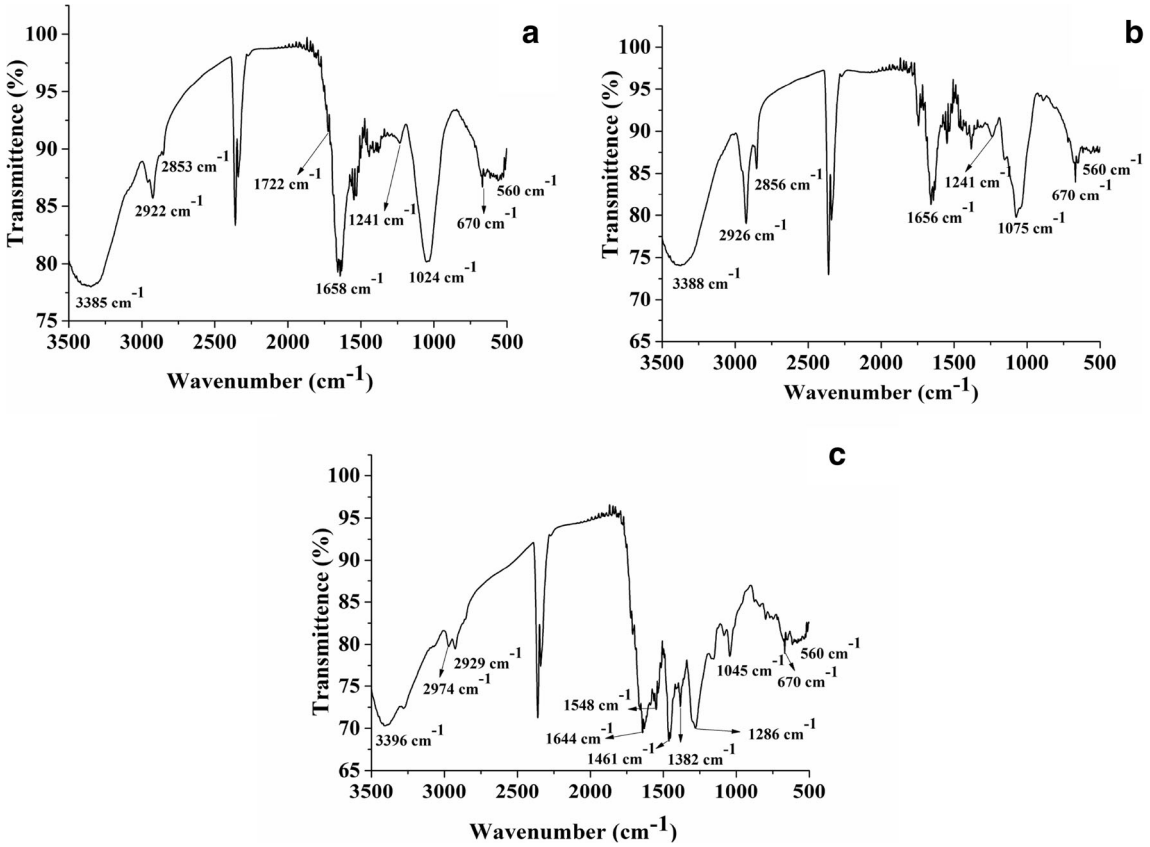

Fig. 6 FTIR spectra of iron oxide nanoparticles synthesized by fungal isolates. **a** STSP10 (*Trichoderma asperellum*). **b** STSP 19 (*Phialemoniopsis ocularis*). **c** STSP 27 (*Fusarium incarnatum*)

(Figs. 7 and 8). The diameter of the IONPs were measured and found to be in a range between 18 and 32 nm for *T. asperellum*, 08–22 nm for *P. ocularis*, and 15–55 nm for *F. incarnatum*, respectively. The SAED pattern for the synthesised IONPs had shown polycrystalline nature for *T. asperellum* and *P. ocularis*. The diffraction ring pattern for IONPs synthesised by *T. asperellum* were (110), (202) and (113) and by *P. ocularis* were (104), (018) and (006). These diffraction patterns were identical for the calculated *d* values for the compound Fe_2O_3 (JCPDS Card No. 33-0664). IONPs synthesised using *F. incarnatum* had showed diffused ring pattern during the SAED analysis. This indicated the amorphic nature of the nanoparticles, which might have occurred due to physical and chemical factors involved during the green synthesis of IONPs. According to a previous report, low pH [58] and high temperature [59] favours the crystallization of nanoparticles. So, during the formation of IONP constant reaction, parameters like pH (3.2 ± 0.02) and temperature (30 °C) might favour the generation of crystalline IONPs, synthesised using *T. asperellum* and *P. ocularis*, whereas maintaining the similar condition might results in amorphisation of IONPs generated using *F. incarnatum*. Thus, it could be concluded that lowering the pH and increasing the temperature during the reaction of FCF with precursor salt might result in the crystallization of IONPs synthesised using *F. incarnatum* [60, 61]. As per classical step- rule scenario [60] crystallization of nanoparticle from solution occurs due to aggregation of atoms/molecules to form amorphous bulk phase. Crystalline phase later appears after nucleation event of nanoparticle in the solution in due course of time. In case of IONPs synthesised using *F. incarnatum* particles, they might not undergo nucleation step thus amorphic bulk phase prevails in the system [60, 61]. Analogously, the crystallization of nanoparticle might occur directly without any amorphous bulk phase [62], which could be observed in the IONPs synthesised using *T. asperellum* and *P. ocularis*. The mean diameter and the standard deviation of the particle was found to be 25 ± 3.94 nm for *T. asperellum*, 13.13 ± 4.32 nm for *P. ocularis* and 30.56 ± 8.68 nm for *F. incarnatum*. The calculated polydispersity index (PDI) for the IONPs synthesised using *T. asperellum*, *P. ocularis* and *F. incarnatum* was found to be 0.02, 0.10 and 0.08 clearly indicating the monodisperse nature of the nanoparticles [47, 62]. TEM images also confirmed the imbeddedment of the synthesised IONPs with a matrix-like structure, which could be the protenecious materials secreted by the fungal strains [29]. IONPs are appeared to be well separated, as they are capped by the protein secreted by the fungal strains. Such smaller size of the synthesised IONPs provides novelty to the work.

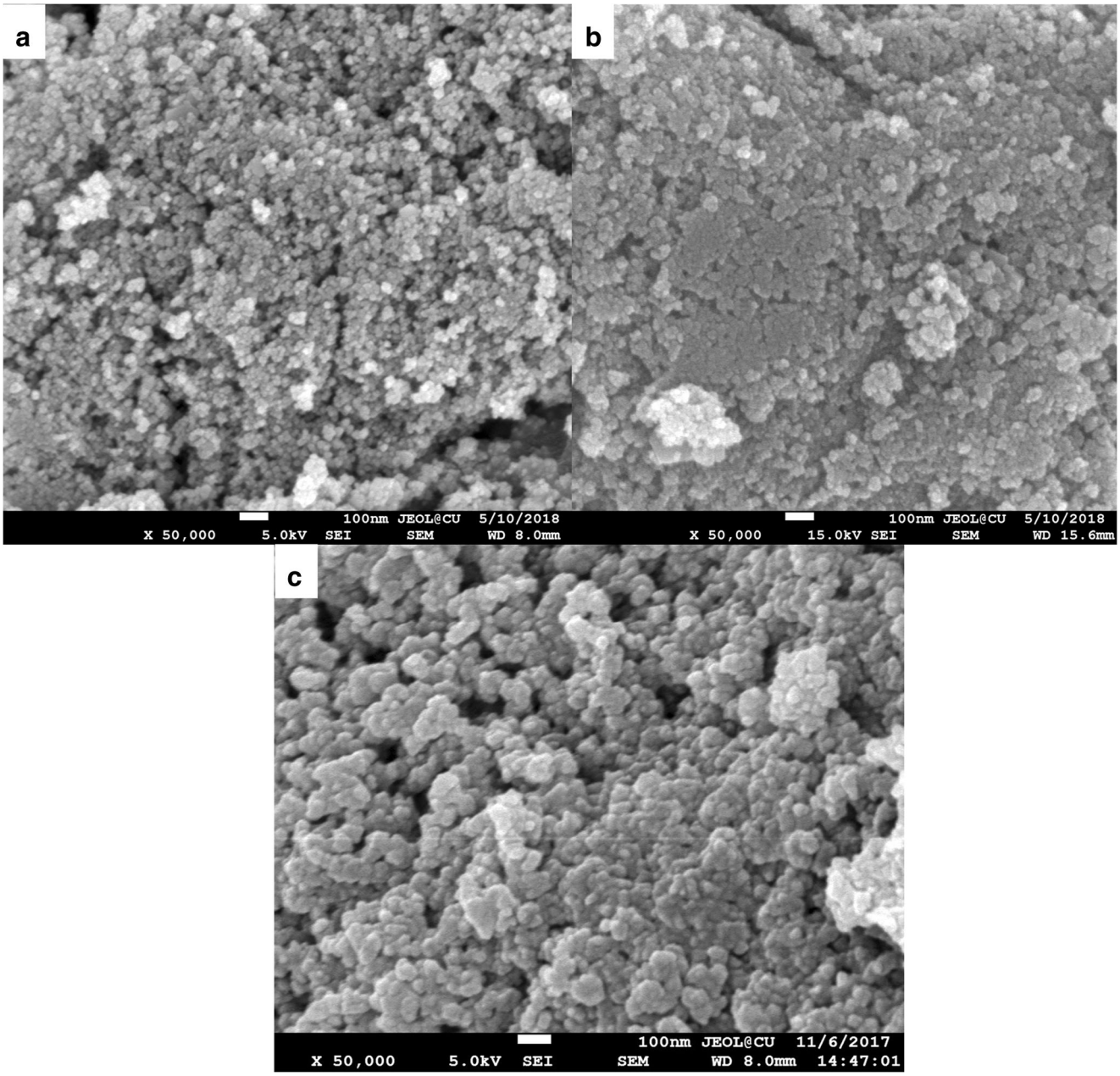

Fig. 7 FESEM micrograph displaying surface topology of iron oxide nanoparticles synthesized by fungal isolates. **a** STSP10 (*Trichoderma asperellum*). **b** STSP 19 (*Phialemoniopsis ocularis*). **c** STSP 27 (*Fusarium incarnatum*)

3.2.4 EDX of Iron Oxide Nanoparticles

To understand the elemental composition of the synthesised IONPs, EDX spectrum were taken for the lyophilised powder sample of IONPs (Fig. 9). The EDX spectrum of the lyophilised IONPs synthesised using isolates *T. asperellum*, *P. ocularis* and *F. incarnatum* had shown strong signal of iron (Fe). The signal of platinum (Pt) and carbon (C) was also observed due to platinum coating and carbon tape. The presence high peak of oxygen (O) characterise the IONPs powder is in oxide form. The absorbance peak of IONPs were approximately in 1 and 7 keV due to surface plasmon resonance of iron nanocrystal [63]. However, several other peaks for Mn and K in EDX spectrum suggest presence of protein precipitate [64].

3.2.5 XRD Analysis

To understand the crystalline nature of IONPs, XRD analysis was performed (Fig. 10). XRD pattern for IONPs synthesised using fungal isolate *T. asperellum* showed distinct diffraction peaks at (012), (104), (110),

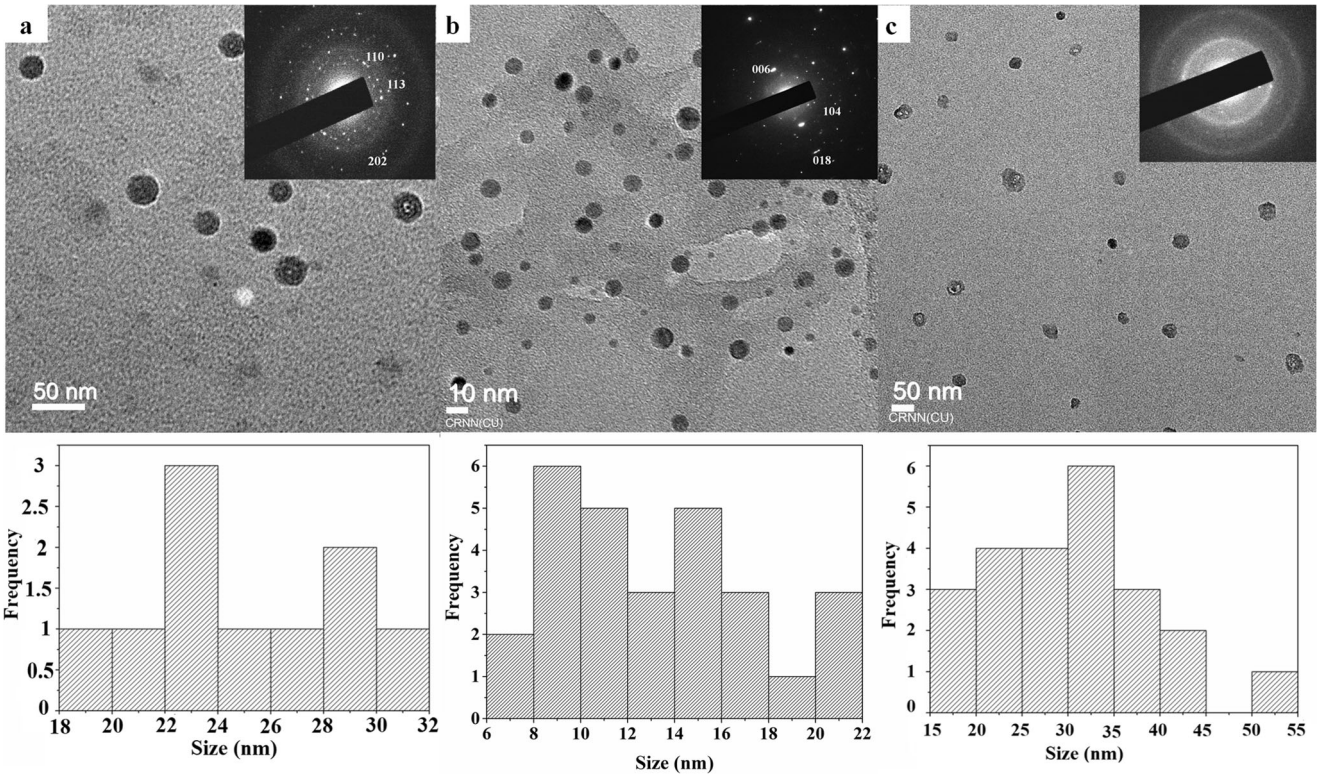

Fig. 8 TEM micrograph revealed the size and shape of mycosynthesized iron oxide nanoparticles. SAED pattern (right upper) and particle size distribution histogram (right lower) showed that average size of iron oxide nanoparticles synthesized by fungal isolates. **a** STSP10 (*Trichoderma asperellum*). **b** STSP 19 (*Phialemoniopsis ocularis*). **c** STSP 27 (*Fusarium incarnatum*)

(202), (024), (116), (214) and (300) lattice plan from $2\theta = 24.31°$, 33.31°, 35.78°, 41.01°, 49.59°, 54.18°, 62.61° and 64.17° for *P. ocularis* diffraction peaks can be observed at (110), (202), (122) and (214) lattice plan from $2\theta = 30°$, 35°, 43° and 63° were consistent with the standard structure of Fe_2O_3 (JCPDS Card No. 33-0664). Several distinct diffraction reflections were seen in the observed XRD pattern which are well matched with the rhombohedral Fe_2O_3 structures with calculated lattice constants of $a = 5.0356$ Å and $c = 13.7489$ Å. In addition to this, due to sharp and strong diffraction reflection, one could confirm that, green-synthesised nanoparticles were well-crystalline. The broadened peak (full width at half maximum) shows the size of both the IONPs synthesised by *T. asperellum* and *P. ocularis* were in nanometre range. Utilising the calculation of average crystalline size from Scherrer formula:

$$d = 0.9\gamma/\beta\cos\theta$$

where d is average crystalline size, γ is wavelength of radiation AND β is the full width at the half maximum at diffraction angle θ. Using THE above equation, it was found that the size of IONPs synthesised by STSP10 and STSP 19 at $2\theta = 33.81°$ was approximately 25 nm and at $2\theta = 35°$ was approximately 15 nm, respectively.

Whereas the IONPs synthesised using *F. incarnatum* does not show any distinctive diffraction peaks. This infer to its amorphic nature of green synthesised nanoparticle.

3.2.6 Comparison with Contemporary Literature

Studies considered for the comparison of different synthesis process are listed in Table 1. Physical and chemical synthesis and green synthesis of IONPs with their size and morphology of the nanoparticle formed were considered in the present comparative study. Different species of plant, fungi, bacteria and algae had been considered under green synthesis processes. From previous studies as represented in Table 1, sonolysis [66], microwave irradiation [72] and flow injection technique [70] had generated spherical-shaped nanoparticles of size less than 10 nm. Among different green synthesis processes plant extract of *Aloe vera* [73], *Salvia officinalis* [75], and fungal extract of *A. alternata* [26] had shown potentiality in reduction of iron salts and generated nanoparticles of size range less than 10 nm. Considering the above-mentioned points, the present study highlights the green synthesis of IONPs by three manglicolous fungi from Indian Sundarban. To our knowledge, it is the first report where manglicolous fungi were utilised for the green synthesis of IONPs. Although in the present study *P. ocularis* had generated nanoparticles of size

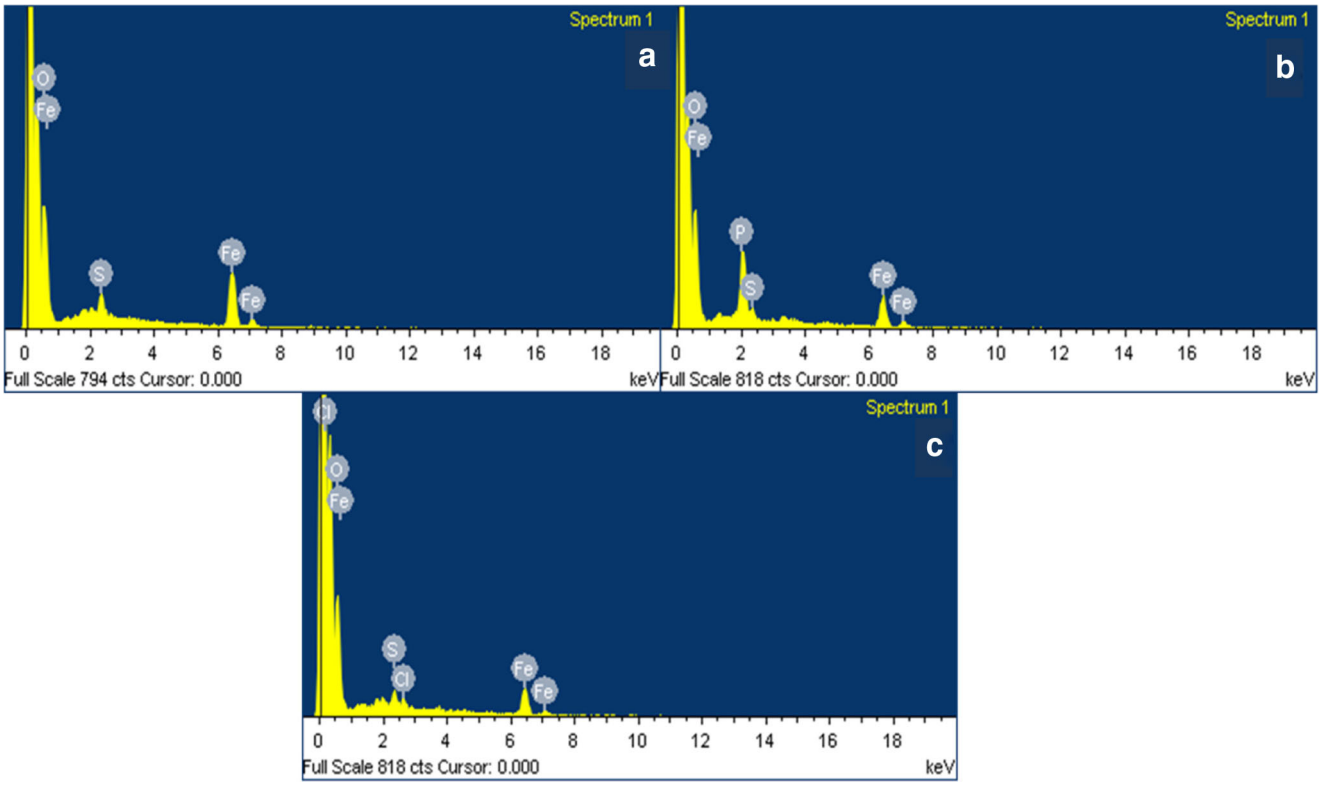

Fig. 9 EDAX Spectrum revealed the chemical composition of iron oxide nanoparticles synthesized by fungal isolates. **a** STSP10 (*Trichoderma asperellum*). **b** STSP 19 (*Phialemoniopsis ocularis*). **c** STSP 27 (*Fusarium incarnatum*)

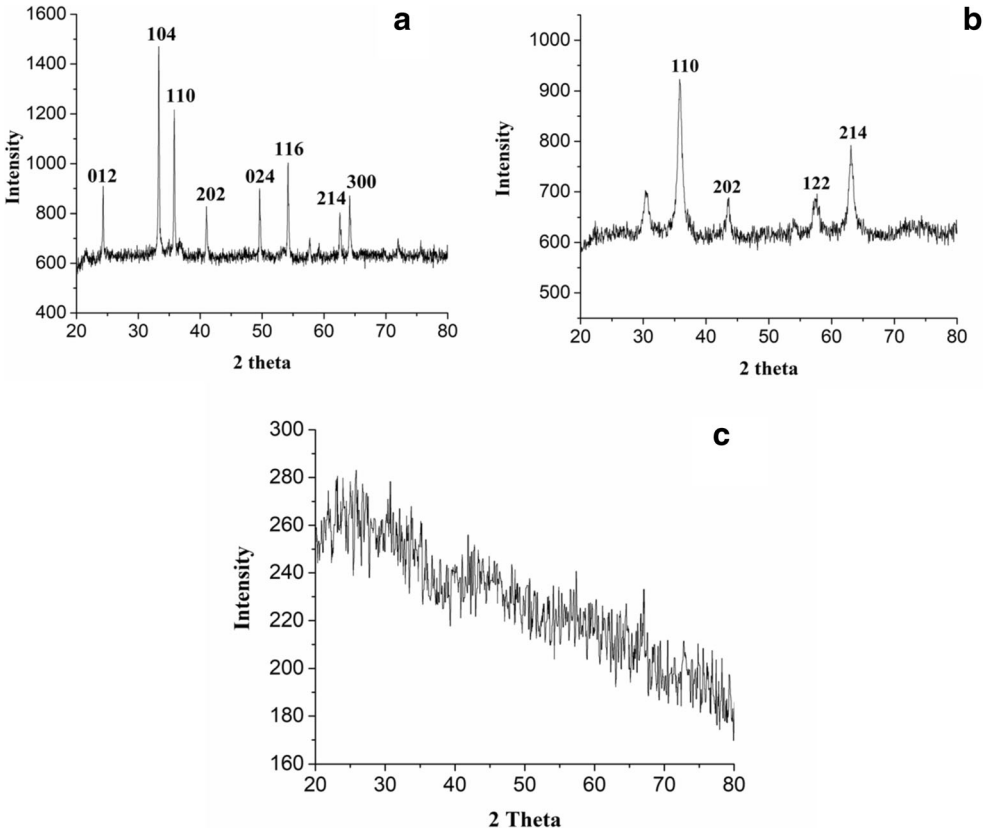

Fig. 10 XRD pattern of iron oxide nanoparticles synthesized by fungal isolates. **a** STSP10 (*Trichoderma asperellum*). **b** STSP 19 (*Phialemoniopsis ocularis*). **c** STSP 27 (*Fusarium incarnatum*)

Table 1 Comparative analysis for the synthesis of IONPs by different processes

Synthesis method		Processes/species	Size	Shape	References
Physical and chemical methods		Liquid phase method	30–100 nm	Spherical	[65]
		Sonolysis	3 nm	Spherical	[66]
		Hydrothermal reaction	27.4 ± 7 nm	Rhombic	[67]
		Polyols method	100 nm	Spherical	[68]
		Chemical precipitation	~ 60 nm	Spherical	[69]
		Flow injection technique	2–7 nm	Spherical	[70]
		Electrochemical method	5–40 nm	Spherical	[71]
		Microwave irradiation	> 10 nm	Spherical	[72]
Green synthesis	Plants	*Azadirachta indica*	50–100 nm	Spherical	[23]
		Aloe vera	6–30 nm	Cubical	[73]
		Eucalyptus globules	50–80 nm	Spherical	[74]
		Salvia officinalis	5–25 nm	Spherical	[75]
	Fungi	*Fusarium oxysporum* and *Verticillium* sp.	20–50 nm	Spherical and cubical	[29]
		Pochonia chlamydosporium, Aspergillus fumigatus, Curvularia lunata, Chaetomium globosum, A. fumigatus, and *A. wentii*	5–200 nm	Spherical	[76]
		Aspergillus sp.	5–200 nm	Spherical	[77]
		Aspergillus japonicus	60–70 nm	Cubical	[31]
		Alternaria alternata	~ 9 nm	Spherical	[26]
		Trichoderma asperellum	18–32 nm	Spherical	Present study
		Phialemoniopsis ocularis	6–22 nm	Spherical	Present study
		Fusarium incarnatum	15–55 nm	Spherical	Present study
	Bacteria	*Actinobacter* sp.	10–40 nm	Cubical	[25]
		Bacillus subtilis	60–80 nm	Spherical	[78]
	Algae	*Sargassum muticum*	14–22 nm	Spherical	[79]

less than 10 nm, but in comparison to other studies, *T. asperellum* and *F. incarnatum* had also generated novel nanoparticles (less than 55 nm).

4 Conclusion

With growing awareness, green synthesis of nanoparticle is becoming a critical interesting topic for researchers of basic and applied science [3]. Green synthesis processes are presenting an alternative solution for the easy, effective, economic, eco-friendly and sustainable way for the development of novel metallic nanoparticles [18–21]. Although there are several routes for the synthesis of nanoparticles but among them mycosynthesis of nanoparticles could be considered as an effective pathway for the development of novel nanoparticles [29]. In the present study, as per our knowledge, we have demonstrated the first report on the green synthesis of IONPs by manglicolous fungi isolated from soil sample of Indian Sundarbans. The mycoreduction of mixture of iron chloride salt had yielded novel monodisperse and stable nanoparticle of range between 25 ± 3.94 nm, 13.13 ± 4.32 nm and 30.56 ± 8.68 nm using *T. asperellum*, *P. ocularis*, and *F. incarnatum*, respectively. IONPs generated using *T. asperellum*, *P. ocularis* showed crystalline nature whereas the IONPs generated using *F. incarnatum* showed amorphic nature. Thus, the present work illustrates the extracellular mycosynthesis and stabilization of IONPs by different bioactive molecules present in the FCF. The advantages of following this protocol over the different protocols present are that the nanoparticles which are formed are quite stable in nature. The longer incubation period of the fungi provides more extracellular protein in FCF, which increases the hydrolysis potentiality of the iron chloride complexes and thus leads to rapid extracellular development of nanoparticles. Hence, the present study revolves around development of green synthesis process which is economic, safer, and environment friendly in nature. Green production of nanoparticle is a novel approach due to its potential applications in different fields like medicine, industry, and waste water treatment. Additionally,

utilization of manglicolous fungi from Indian Sundarbans for bioreduction opens up several avenues for research on mangrove fungi. Further studies on the biochemistry of the extracellular protein matrix of fungal cell filtrate are needed to understand the mechanism of the bioreduction procedure. Cataloguing the biomolecules responsible for the reduction of iron salt complex can leads to development of improved green process. Thus, in the near future, manglicolous fungi could be utilised as nanofactories for production of metal nanocrystals of complex structure and controlled able size.

Funding The authors are thankful to Department of Biotechnology (DBT), India (No. BT/PR9465/NDB/39/360/2013) and Centre for Nanoscience and Nanotechnology (CRNN), University of Calcutta, for financial and infrastructural support.

Compliance with Ethical Standards

Conflict of Interest None.

Research Involving Humans and Animals Statement None.

Informed Consent None.

Funding Statement None.

References

1. Elghanian, R., Storhoff, J. J., Mucic, R. C., Letsinger, R. L., & Mirkin, C. A. (1997). Selective colorimetric detection of polynucleotides based on the distance-dependent optical properties of gold nanoparticles. *Science, 277*, 1078–1081.
2. Luechinger, N. A., Grass, R. N., Athanassiou, E. K., & Stark, W. J. (2010). Bottom-up fabrication of metal/metal nanocomposites from nanoparticles of immiscible metals. *Chemistry of Materials, 22*, 155–160.
3. Bakshi, M., Ghosh, S., & Chaudhuri, P. (2015). Green synthesis, characterization and antimicrobial potential of sliver nanoparticles using three mangrove plants from Indian Sundarban. *Bionanoscience, 5*, 162–170.
4. Thanh, N. T., & Green, L. A. (2010). Functionalisation of nanoparticles for biomedical applications. *Nano Today, 5*, 213–230.
5. Atabaev, T. S. (2018). PEG-coated superparamagnetic dysprosium-doped Fe3O4 nanoparticles for potential MRI imaging. *Bionanoscience, 8*, 299–303.
6. Li, Z., Kawashita, M., Araki, N., Mitsumori, M., & Hiraoka, M. (2009). Preparation of size-controlled magnetite nanoparticles for hyperthermia of cancer. *Transactions of the Materials Research Society of Japan, 34*, 77–80.
7. Lin, K. S., Chang, N. B., & Chuang, T. D. (2008). Fine structure characterization of zero-valent iron nanoparticles for decontamination of nitrites and nitrates in wastewater and groundwater. *Science and Technology of Advanced Materials, 9*, 025015.
8. Gui, M., Smuleac, V., Ormsbee, L. E., Sedlak, D. L., & Bhattacharyya, D. (2012). Iron oxide nanoparticle synthesis in aqueous and membrane systems for oxidative degradation of tri chloro ethylene from water. *Journal of Nanoparticle Research, 14*, 861.
9. Ingle, A., Rai, M., Gade, A., & Bawaskar, M. (2009). *Fusarium solani:* a novel biological agent for the extracellular synthesis of silver nanoparticles. *Journal of Nanoparticle Research, 11*, 2079.
10. Mallik, K., Witcomb, M. J., & Scurell, M. S. (2005). Redox catalytic property of gold nanoclusters: evidence of an electron-relay effect. *Applied Physics A: Materials Science & Processing, 80*, 797–801.
11. Liz-Marzan, L. (2006). Tailoring surface plasmons through the morphology and assembly of metal nanoparticles. *Langmuir, 22*, 32–41.
12. Fedlheim, D. L., & Foss, C. A. (2001). *Metal nanoparticles: synthesis, characterization, and applications*. Boca Raton: CRC Press.
13. Kamat, P. V. (1993). Photochemistry on nonreactive and reactive (semiconductor) surfaces. *Chemical Reviews, 93*, 267–300.
14. Giguere, R. J., Bray, T. L., Duncan, S. M., & Majetich, G. (1986). Application of commercial microwave ovens to organic synthesis. *Tetrahedron Letters, 27*, 4945–4948.
15. Park, S. J., Kim, S., Lee, S., Khim, Z. G., Char, K., & Hyeon, T. (2000). Synthesis and magnetic studies of uniform iron nanorods and nanospheres. *Journal of the American Chemical Society, 122*(35), 8581–8582.
16. Sun, S., & Zeng, H. (2002). Size-controlled synthesis of magnetite nanoparticles. *JACS, 124*, 8204–8205.
17. Goya, G. F., Berquo, T. S., Fonseca, F. C., & Morales, M. P. (2003). Static and dynamic magnetic properties of spherical magnetite nanoparticles. *Journal of Applied Physics, 94*, 3520–3528.
18. Palomo, J., & Filice, M. (2016). Biosynthesis of metal nanoparticles: novel efficient heterogeneous nanocatalysts. *Nanomaterials, 6*, 84.
19. Bhargava A, Jain N, Panwar J (2011) Synthesis and application of magnetic nanoparticles: a biological perspective. In: Dhingra HK, Jha PN, Bajpai P (eds) *Current topics in biotechnology and microbiology: recent trends*. Lap Lambert Academic Publishing AG & Co Kg, Colne, pp 117–155.
20. Das, P., Mahanty, S., Ganguli, A., Das, P., & Chaudhuri, P. (2019). Role of manglicolous fungi isolated from Indian Sundarban mangrove forest for the treatment of metal containing solution: batch and optimization using response surface methodology. *Environmental Technology and Innovation, 13*, 166–178.
21. Teja, A. S., & Koh, P. Y. (2009). Synthesis, properties, and applications of magnetic iron oxide nanoparticles. *Progress in Crystal Growth and Characterization of Materials, 55*, 22–45.
22. Hoag, G. E., Collins, J. B., Holcomb, J. L., Hoag, J. R., Nadagouda, M. N., & Varma, R. S. (2009). Degradation of bromothymol blue by 'greener' nano-scale zero-valent iron synthesized using tea polyphenols. *Journal of Materials Chemistry, 19*, 8671–8677.
23. Pattanayak, M., & Nayak, P. L. (2013). Green synthesis and characterization of zero valent iron nanoparticles from the leaf extract of Azadirachta indica (Neem). *World Journal of Nano Science & Technology, 2*(1), 06–09.
24. Rao, A., Bankar, A., Kumar, A. R., Gosavi, S., & Zinjarde, S. (2013). Removal of hexavalent chromium ions by Yarrowia lipolytica cells modified with phyto-inspired Fe^0/Fe_3O4 nanoparticles. *Journal of Contaminant Hydrology, 146*, 63–73.
25. Bharde, A., Wani, A., Shouche, Y., Joy, P. A., Prasad, B. L., & Sastry, M. (2005). Bacterial aerobic synthesis of nanocrystalline magnetite. *JACS, 127*, 9326–9327.
26. Mohamed, Y. M., Azzam, A. M., Amin, B. H., & Safwat, N. A. (2015). Mycosynthesis of iron nanoparticles by *Alternaria alternata* and its antibacterial activity. *African Journal of Biotechnology, 14*, 1234–1241.
27. Subramaniyam, V., Subashchandrabose, S. R., Thavamani, P., Megharaj, M., Chen, Z., & Naidu, R. (2015). *Chlorococcum* sp. MM11—a novel phyco-nanofactory for the synthesis of iron nanoparticles. *Journal of Applied Phycology, 27*, 861–1869.

28. Gade, A., Ingle, A., Whiteley, C., & Rai, M. (2010). Mycogenic metal nanoparticles: progress and applications. *Biotechnology Letters, 32*, 593–600.
29. Bharde, A., Rautaray, D., Bansal, V., Ahmad, A., Sarkar, I., Yusuf, S. M., & Sastry, M. (2006). Extracellular biosynthesis of magnetite using fungi. *Small, 2*, 135–141.
30. Tarafdar, J. C., & Raliya, R. (2013). Rapid, low-cost, and ecofriendly approach for iron nanoparticle synthesis using *Aspergillus oryzae* TFR9. *Journal of Nanoparticles.* https://doi.org/10.1155/2013/141274.
31. Bhargava, A., Jain, N., Barathi, M., Akhtar, M. S., Yun, Y. S., & Panwar, J. (2013). Synthesis, characterization and mechanistic insights of mycogenic iron oxide nanoparticles. *Journal of Nanoparticle Research, 15*, 2031.
32. Kathiresan, K., Manivannan, S., Nabeel, M. A., & Dhivya, B. (2009). Studies on silver nanoparticles synthesized by a marine fungus, *Penicillium fellutanum* isolated from coastal mangrove sediment. *Colloids and Surfaces. B, Biointerfaces, 71*, 133–137.
33. Saha, S., Sarkar, J., Chattopadhyay, D., Patra, S., Chakraborty, A., et al. (2010). Production of silver nanoparticles by a phytopathogenic fungus *Bipolaris nodules* and its antimicrobial activity. *Digest Journal of Nanomaterials and Biostructures, 5*, 887–895.
34. Sarkar, J., Chattopadhyay, D., Patra, S., Deo, S. S., Sinha, S., et al. (2011a). *Alternaria alternata* mediated synthesis of protein capped silver nanoparticles and their genotoxic activity. *Digest Journal of Nanomaterials and Biostructures, 6*, 563–573.
35. Sridhar K R (2013) Mangrove fungal diversity of west coast of India. Mangroves of India: their biology and uses, 161–182.
36. Gopal, B., & Chauhan, M. (2006). Biodiversity and its conservation in the Sundarban mangrove ecosystem. *Aquatic Sciences, 68*, 338–354.
37. Hyde, K. D., & Jones, E. B. G. (1988). Marine mangrove fungi. *Marine Ecology, 9*, 15–33. https://doi.org/10.1111/j.1439-0485.1988.tb00196.x.
38. Jones, E. B. G. (2000). Marine fungi: some factors influencing biodiversity. *Fungal Diversity, 4*, 53–73.
39. Kohlmeyer, J., & Kohlmeyer, E. (1979). *Marine mycology. The higher fungi*. New York: Academic Press.
40. Findlay, S., Smith, P. J., & Meyer, J. L. (1986). Effect of detritus addition on metabolism of river sediment. *Hydrobiologia, 137*, 257–263.
41. Barnett, H. L., & Hunter, B. B. (1972). *Illustrated genera of imperfect fungi*. Minneapolis: Burgess publishing company.
42. Domsch, K. H., Gams, W., & Anderson, T. H. (1980). *Compandium of soil fungi. Vols. 1 and 2*. London: Academic Press.
43. Watanabe T (2010) *Pictorial atlas of soil and seed fungi: morphologies of cultured fungi and key to species*. CRC press.
44. Aamir, S., Sutar, S., Singh, S. K., & Baghela, A. (2015). A rapid and efficient method of fungal genomic DNA extraction, suitable for PCR based molecular methods. *Plant Pathology & Quarantine, 5*, 74–81.
45. White, T. J., Bruns, T., Lee, S., & Taylor, J. (1990). Amplification and direct sequencing of fungal ribosomal RNA genes for phylogenetics. In M. A. Innis, D. H. Gelfand, J. J. Sninsky, & T. J. White (Eds.), *PCR protocols a guide to methods and applications* (pp. 315–322). San Diego: Academic aPress. https://doi.org/10.1016/b978-0-12-372180-8.50042-1.
46. Qin, Z., Joo, J., Gu, L., & Sailor, M. J. (2014). Size control of porous silicon nanoparticles by electrochemical perforation etching. *Particle and Particle Systems Characterization, 31*, 252–256.
47. Kozlov, N. K., Natashina, U. A., Tamarov, K. P., Gongalsky, M. B., et al. (2017). Recycling of silicon: From industrial waste to biocompatible nanoparticles for nanomedicine. *Mater Res Express, 4*, 095026.
48. Gottimukkala, K. S. V. (2017). Green synthesis of iron nanoparticles using green tea leaves extract. *Journal of Nanomedicine & Biotherapeutic Discovery, 7*, 151. https://doi.org/10.4172/2155-983X.1000151.
49. Mazumdar, H., & Haloi, N. (2017). A study on biosynthesis of iron nanoparticles by *Pleurotus* sp. *Journal of Microbiology and Biotechnology Research, 1*, 39–49.
50. Basu, S., & Chakravorty, D. (2006). Optical properties of nanocomposites with iron core–iron oxide shell structure. *Journal of Non-Crystalline Solids, 352*, 380–385.
51. Guo, L., Huang, Q., Li, X. Y., & Yang, S. (2001). Iron nanoparticles: synthesis and applications in surface enhanced Raman scattering and electrocatalysis. *Physical Chemistry Chemical Physics, 3*, 1661–1665.
52. Morgada, M. E., Levy, I. K., Salomone, V., Farías, S. S., López, G., & Litter, M. I. (2009). Arsenic (V) removal with nanoparticulate zerovalent iron: effect of UV light and humic acids. *Catalysis Today, 143*, 261–268.
53. Namduri, H., & Nasrazadani, S. (2008). Quantitative analysis of iron oxides using Fourier transform infrared spectrophotometry. *Corrosion Science, 50*, 2493–2497.
54. Macdonald, I. D. G., & Smith, W. E. (1996). Orientation of cytochrome c adsorbed on a citrate-reduced silver colloid surface. *Langmuir, 12*, 706–713.
55. Yang, T., Li, Z., Wang, L., Guo, C., & Sun, Y. (2007). Synthesis, characterization, and self-assembly of protein lysozyme monolayer-stabilized gold nanoparticles. *Langmuir, 23*, 10533–10538.
56. Rangnekar, A., Sarma, T. K., Singh, A. K., Deka, J., Ramesh, A., & Chattopadhyay, A. (2007). Retention of enzymatic activity of α-amylase in the reductive synthesis of gold nanoparticles. *Langmuir, 23*, 5700–5706.
57. Wang, Y., Maksimuk, S., Shen, R., & Yang, H. (2007). Synthesis of iron oxide nanoparticles using a freshly-made or recycled imidazolium-based ionic liquid. *Green Chemistry, 9*, 1051–1056.
58. El-Lateef, H. M. A., Touny, A. H., & Saleh, M. M. (2018). Synthesis of crystalline and amorphous iron phosphate nanoparticles by simple low-temperature method. *Materials Research Express, 6*(3), 035030.
59. Kappes, B. B., Meacham, B. E., Tang, Y. L., & Branagan, D. J. (2003). Relaxation, recovery, crystallization, and recrystallization transformations in an iron-based amorphous precursor. *Nanotechnology, 14*, 1228.
60. Baumgartner, J., Dey, A., Bomans, P. H., et al. (2013). Nucleation and growth of magnetite from solution. *Nature Materials, 12*, 310.
61. Thanh, N. T., Maclean, N., & Mahiddine, S. (2014). Mechanisms of nucleation and growth of nanoparticles in solution. *Chemical Reviews, 114*, 7610–7630.
62. Nidhin, M., Indumathy, R., Sreeram, K. J., & Nair, B. U. (2008). Synthesis of iron oxide nanoparticles of narrow size distribution on polysaccharide templates. *Bulletin of Materials Science, 31*, 93–96.
63. Shahwan, T., Sirriah, S. A., Nairat, M., Boyacı, E., Eroğlu, A. E., & Scott TB Hallam, K. R. (2011). Green synthesis of iron nanoparticles and their application as a Fenton-like catalyst for the degradation of aqueous cationic and anionic dyes. *Chemical Engineering Journal, 172*, 258–266.
64. Hashimoto, H., Yokoyama, S., Asaoka, H., et al. (2007). Characteristics of hollow microtubes consisting of amorphous iron oxide nanoparticles produced by iron oxidizing bacteria, *Leptothrix ochracea*. *Journal of Magnetism and Magnetic Materials, 310*, 2405–2407.
65. Sugimoto, T., & Matijević, E. (1980). Formation of uniform spherical magnetite particles by crystallization from ferrous hydroxide gels. *Journal of Colloid and Interface Science, 74*, 227–243.
66. Hasany, S. F., Ahmed, I., Rajan, J., & Rehman, A. (2012). Systematic review of the preparation techniques of iron oxide magnetic nanoparticles. *Nanoscience and Nanotechnology, 2*, 148–158. https://doi.org/10.5923/j.nn.20120206.01.

67. Xu, H., Wang, X., & Zhang, L. (2008). Selective preparation of nanorods and micro-octahedrons of Fe2O3 and their catalytic performances for thermal decomposition of ammonium perchlorate. *Powder Technology, 185*, 176–180.
68. Joseyphus, R. J., Shinoda, K., Kodama, D., & Jeyadevan, B. (2010). Size controlled Fe nanoparticles through polyol process and their magnetic properties. *Materials Chemistry and Physics, 123*, 487–493.
69. Wu, S., Sun, A., Zhai, F., Wang, J., Xu, W., Zhang, Q., & Volinsky, A. A. (2011). Fe_3O_4 magnetic nanoparticles synthesis from tailings by ultrasonic chemical co-precipitation. *Materials Letters, 65*(12), 1882–1884.
70. Salazar-Alvarez, G., Muhammed, M., & Zagorodni, A. A. (2006). Novel flow injection synthesis of iron oxide nanoparticles with narrow size distribution. *Chemical Engineering Science, 61*, 4625–4633.
71. Starowicz, M., Starowicz, P., Żukrowski, J., Przewoźnik, J., et al. (2011). Electrochemical synthesis of magnetic iron oxide nanoparticles with controlled size. *Journal of Nanoparticle Research, 13*, 7167–7176.
72. Hu, X., Yu, J. C., Gong, J., Li, Q., & Li, G. (2007). α-Fe2O3 nanorings prepared by a microwave-assisted hydrothermal process and their sensing properties. *Advanced Materials, 19*, 2324–2329.
73. Phumying, S., Labuayai, S., Thomas, C., Amornkitbamrung, V., Swatsitang, E., & Maensiri, S. (2013). Aloe vera plant-extracted solution hydrothermal synthesis and magnetic properties of magnetite (Fe3O4) nanoparticles. *Applied Physics A, 111*(4), 1187–1193.
74. Madhavi, V., Prasad, T. N., et al. (2013). Application of phytogenic zerovalent iron nanoparticles in the adsorption of hexavalent chromium. *Spectrochimica Acta A, 116*, 17–25.
75. Wang, Z., Fang, C., & Mallavarapu, M. (2015). Characterization of iron–polyphenol complex nanoparticles synthesized by sage (*Salvia officinalis*) leaves. *Environmental Technology and Innovation, 4*, 92–97.
76. Kaul, R. K., Kumar, P., Burman, U., Joshi, P., et al. (2012). Magnesium and iron nanoparticles production using microorganisms and various salts. *Materials Science - Poland, 30*, 254–258.
77. Pavani, K. V., & Kumar, N. S. (2013). Adsorption of iron and synthesis of iron nanoparticles by *Aspergillus* species kvp 12. *Am J Nanomater, 1*, 24–26.
78. Sundaram, P. A., Augustine, R., & Kannan, M. (2012). Extracellular biosynthesis of iron oxide nanoparticles by *Bacillus subtilis* strains isolated from rhizosphere soil. *Biotechnology and Bioprocess Engineering, 17*(4), 835–840.
79. Mahdavi, M., Namvar, F., Ahmad, M. B., & Mohamad, R. (2013). Green biosynthesis and characterization of magnetic iron oxide (Fe_3O_4) nanoparticles using seaweed (*Sargassum muticum*) aqueous extract. *Molecules, 18*, 5954–5964.